

OPTIMAL SEED PLANTING FOR GROWTH-REGULATED NANOMANUFACTURING

Shaghayegh Abbasi¹, Sathana Kitayaporn², Daniel T. Schwartz², and Karl F. Böhringer¹

¹Department of Electrical Engineering, ²Department of Chemical Engineering
University of Washington, Seattle, WA, USA

ABSTRACT

We develop, model, and optimize a growth-regulated nanomanufacturing method which is more flexible and cost-effective than conventional serial nanomanufacturing methods. An automated system is designed which takes a geometric representation of an object as the input, produces the growth-initiating “seed” positions for entry to fabrication tools, and gives the grown object as the output. Electron beam lithography is used to fabricate gold seeds, which is followed by copper deposition via electroplating. To improve the structure precision, we first present a model for seed-initiated material growth based on Green’s function calculations. This model is then used to develop an algorithm for optimal seed planting to produce the highest accuracy object with the fewest number of tool moves. Both the model and the optimization algorithm are validated by experimental results.

1. INTRODUCTION

Nanotechnology has become increasingly important recently due to its expected high impact on health, environment, energy, and many other aspects. In electronics, for instance, nanotechnology is useful in increasing the density of components, decreasing the cost, and increasing the performance per device and per integrated circuit [1]. The key attributes in any nanomanufacturing process consist of cost, flexibility, quality, time, and precision [2]. Here we offer a fully automated method for manufacturing micro and nano structures which reduces cost and process time compared to conventional serial manufacturing methods, without threatening the attributes of flexibility and quality. In addition, we propose methods for optimizing the structure precision.

Pattern creation is usually the most expensive and time consuming step in nanomanufacturing since it often relies on serial rate tools, e.g. electron beam lithography (EBL) and dip-pen lithography. An efficient solution for time and cost reduction is planting growth-initiating “seeds” only at selected locations (just a fraction of the total object area) for patterning. In biomimetic synthesis, for example, inorganic synthesizing polypeptides (ISPs) are used as seeds to bind and synthesize technologically important materials [3]. This method has several advantages such as unparalleled control over material composition and crystallinity, mild aqueous processing

conditions, and the integration of bottom-up self-assembly (using seeds to synthesize inorganic materials) with top-down multi-scale methods for patterning seeds. Here gold is used as the seed material to deposit copper via electrodeposition. The seed patterning is performed using EBL.

The seed positioning determines the output structure precision. The simplest placement strategy for the seeds is a regular square array. However, due to seed overgrowth on sharp corners and on edges, the final precision of such a structure is not optimal. Seed-initiated growth is modeled here using mass flow equilibrium and Green’s function solution of the diffusion equation. The predicted output structure by this model is then compared to the desired structure, and a seed positioning optimization algorithm is implemented to achieve higher precision.

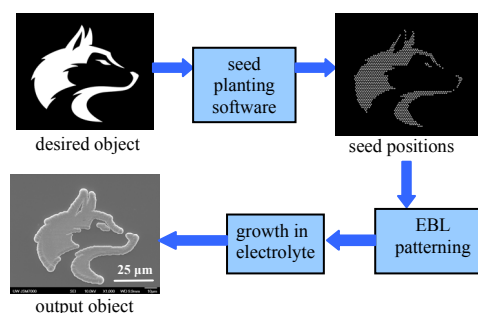


Figure 1: The automated process from inputting the desired object to the growth of the output object: The desired object is first entered in our seed planting software, which outputs the seed positions in the format compatible with EBL. The seeds are fabricated on the substrate using these positions, and then grown using electrodeposition. Finally the grown shape (output object) is shown.

2. MATERIALS AND METHODS

Design Automation

Here we design an automated method which takes a geometric representation of an object as the input, produces the seed positions for entry to fabrication tools, and gives the grown object as the output. First a MATLAB program is used to produce the seed position coordinates based on the geometric representation of the

object, and to convert the coordinates to the format compatible with the EBL tool. The seed positions are then entered in the software connected to the EBL tool, and the seed points are patterned on the substrate. Finally an electroplating process is used to grow the seeds and obtain the output object (Fig. 1). The substrate fabrication and the electroplating process are explained in more detail in the two following sections.

Substrate Fabrication

The fabrication starts with a 4" silicon wafer. In the first step, a Cr/Au layer with 3 nm/50 nm thickness is evaporated on the wafer as seed material, followed by spin-coating a 100 nm thick PMMA layer as photoresist. Next, EBL is used to pattern the seeds, followed by PMMA development in methyl isobutyl ketone (MIBK): isopropanol alcohol (IPA) 1:3 (Fig. 2(a)). The development exposes the gold as the seeds for the following growth step. The seeds are patterned as disks, and their radius ranges from 62 nm to 500 nm.

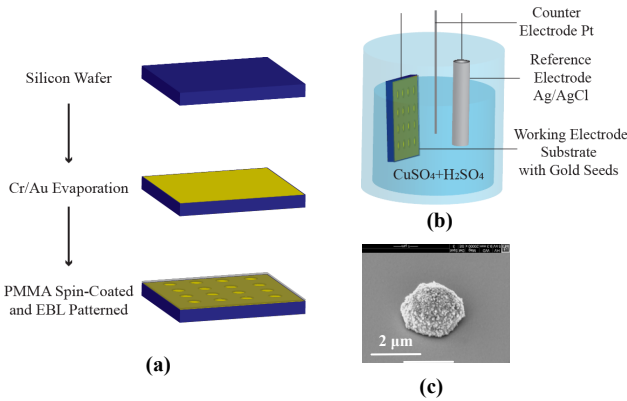


Figure 2: (a) Fabrication process of growth substrate. The seed radius is usually between 62 nm and 500 nm. (b) Copper is grown on the gold seeds via electrodeposition. (c) SEM picture of a single grown seed.

Electroplating Setup

Copper is grown at the patterned seeds via electrodeposition in room temperature using 0.5M CuSO₄ and 0.5M H₂SO₄ at -300 mV vs. Ag/AgCl reference. All experiments are done in a quiescent 40mL single compartment cell with a platinum wire as a counter electrode and an Ag/AgCl saturated KCl reference electrode (Fig. 2(b)). Experimental results show that copper grows in hemispherical shape on the circular seed points (Fig. 2(c)).

3. MODELING AND EXPERIMENTS

Modeling

We first model the growth of a single seed, and then we use this model to simulate the growth of multiple seeds which interact with each other. The mass transfer for a hemispherical growth using electroplating is as follows:

$$\dot{m} = 2\pi MW_{cu} D_{cu^{+2}} C_{cu^{+2}} r \quad (1)$$

where m is the added mass, the dot means the derivative with respect to time, MW_{cu} , $D_{cu^{+2}}$, and $C_{cu^{+2}}$ are the molecular weight, diffusion coefficient and ion concentration of copper, and r is the radius of the growing hemisphere.

On the other hand, using the geometry of the system we can get:

$$\dot{m} = \rho_{cu} \frac{dV}{dt} = 2\rho_{cu} \pi r^2 \frac{dr}{dt} \quad (2)$$

where ρ_{cu} is the density of copper.

Using the mass flow equilibrium [4] and thus equating the right sides of Eq. 1 and Eq. 2 and solving for r , we obtain:

$$r^2 = 2\hat{V}_{cu} D_{cu^{+2}} C_{cu^{+2}} (t - t_0) + r_0^2 \quad (3)$$

where $\hat{V}_{cu} = \frac{MW_{cu}}{\rho_{cu}}$ is called the molar volume, t is the time, and t_0 is the growth start time.

When multiple seeds are growing in an array, the metal ion concentration around each seed is affected by the neighbor seeds. This effect is modeled here using the Green's function solution of the diffusion equation [5]. Since the neighbor seeds act as a sink for the metal ions and decrease the concentration of ions around the seed of interest, the modified concentration around each seed will be calculated as:

$$C_{cu^{+2},new} = C_{cu^{+2}} \left(1 - \sum_i \frac{1}{4\pi d_{i,n}} \right) \quad (4)$$

where $d_{i,n}$ is the normalized distance between the seed and its i^{th} neighbor, and the sigma is used to add together the effect of all neighbors on the seed of interest. The term inside the sigma comes from the diffusion equation. The seed distance needs to be normalized because in the model the seeds are assumed to be point sinks, where in reality they are growing as hemispheres. Hence, the distance is normalized over the size of the seeds, i.e. $2r$. This factor can also be determined using mass transport equations as *diffusion length*+ r , which gives the same result $2r$ [6]. Hence, we will have:

$$d_{i,n} = d_i / 2r \quad (5)$$

where d_i is the distance between the seed and its i^{th} neighbor. Replacing $d_{i,n}$ and C_{cu}^{+2} from Eq. 4 and Eq. 5 in Eq. 3 and solving for r , we get:

$$r = -2\hat{V}_{cu} D_{cu^{+2}} C_{cu^{+2}} (t-t_0) \sum_i \frac{1}{4\pi d_i} + \sqrt{2\hat{V}_{cu} D_{cu^{+2}} C_{cu^{+2}} (t-t_0) + 4\hat{V}_{cu}^2 D_{cu^{+2}}^2 C_{cu^{+2}}^2 (t-t_0)^2 \left(\sum_i \frac{1}{4\pi d_i} \right)^2} + r_0^2 \quad (6)$$

which shows that if the number of neighbors is increased or they become closer to the seed, the growth radius becomes smaller.

Experiments

Two sets of experiments are designed to evaluate the model. In the first set of experiments, the seed design consists of a center seed, surrounded by 0 to 8 neighbor seeds, which are distributed evenly on a circle around the center seed (Fig. 3). The experimental setup is explained in section 2. The seed size is 500 nm, and the spacing between the seed and its neighbors is 10 μm . For each time step samples are grown in the electrolyte and then taken out for measurement. Fig. 3 shows the radius of the grown center seed as a function of time and for different numbers of neighbors. The comparison between experimental results (dots) and the model (red line) supports our model.

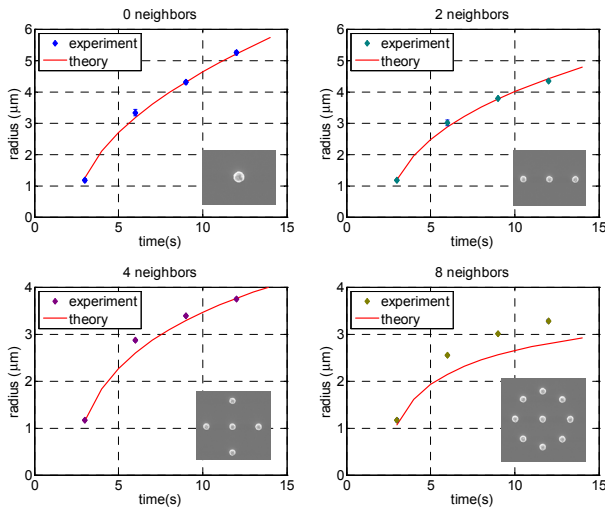


Figure 3: The radius of growing seed with different numbers of neighbors is measured as a function of time in experiments (dots), and is plotted along with the theoretical prediction (red line), which shows good agreement between model and experiments. The error bars on the experimental result show standard deviation for at least 3 experiments, which in some cases is too small to be visible.

In another set of experiments, seed patterns are designed as regular square arrays. Fig. 4(a) shows the model (green circles) and the experimental results (light gray regions), and in Fig. 4(b) model and experiments are being overlaid at different time steps for comparison. It can be seen here that model and experimental results are in good agreement.

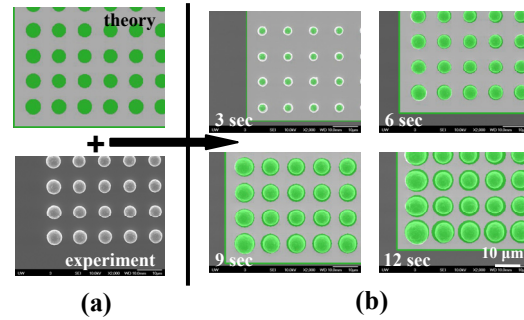


Figure 4: A comparison between theory and experiment is shown for a square array. The simulation and experimental results are shown separately in (a). The two are then overlapped in (b) at different time steps for easy comparison. The green disks show the theory and the light gray regions in the SEM image show the experimental results. The seed size is 500 nm, and the spacing is 10 μm .

4. OPTIMIZATION METHODS

The experimental results of growing desired objects using regular square array seed patterns show that there will be some difference between the output object and the desired object. One reason for this difference is the overgrowth of seeds on the edges and corners of the object due to being exposed to more metal ions compared to the inside seeds. Two controlling factors of the grown seed size are the number and the spacing of neighbors. The effect of initial seed size is negligible in our experiments due to their small size. The edge and corner seeds have lower numbers of neighbors, and thus bigger radii, compared to the middle seeds. To optimize the seed positions, we can make their radii smaller and hence prevent the overgrowth by changing their distance to their neighbors. The edge and corner seeds thus need to be moved by motion vector \vec{M} calculated by the following method.

To calculate the components (Δx , Δy) of the motion vector \vec{M} for each seed two equations are required. The first equation makes use of the desired change in grown radius (Δr). For edge and corner seeds, we define:

$$\Delta r = r_{desired} - r_{seed} \quad (7)$$

where r_{seed} is the grown seed radius calculated from Eq. 6, and $r_{desired}$ is the desired radius. We define the desired

radius as the distance between the edge/corner seed and the edge of the desired object (Fig. 5).

We then use the following equation to find a relationship between Δx and Δy .

$$\Delta r = \frac{\partial r}{\partial x} \times \Delta x + \frac{\partial r}{\partial y} \times \Delta y \quad (8)$$

where derivatives of r with respect to x and y are calculated from Eq. 6.

The second equation relating Δx and Δy is deduced from the direction of motion, defined such that the seed moves towards (away from) the middle point of neighboring seeds for negative (positive) Δr , hence:

$$\Delta y / \Delta x = \left(y_{seed} - \sum_i y_i / n \right) / \left(x_{seed} - \sum_i x_i / n \right) \quad (9)$$

where x_i and y_i are coordinates of each neighbor seed respectively, and n is the number of neighbors. Using Eq. 7, Eq. 8, and Eq. 9, Δx and Δy can be calculated as a function of neighbor positions, and used to design the optimum seed positions. Fig. 6 shows the experimental results of the output object before and after optimization, showing sharper corners and less overgrown area, considerably improving the output.

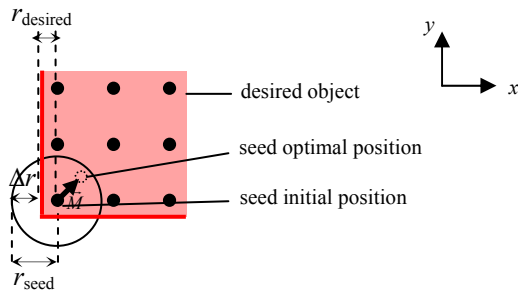


Figure 5: A corner seed growth is shown. The circle shows the grown seed, and the actual and desired radii are demonstrated. The motion vector \vec{M} which results in the optimized seed positioning is calculated by decomposing it into components Δx and Δy .

5. CONCLUSION

We propose a method for nanomanufacturing using growth-regulating seed points. By patterning the seeds only at selected locations, which is only a fraction of total object area, the cost is reduced. For accuracy enhancement, the seed growth is modeled based on Green's function and diffusion equation. It is understood from the model and verified by the experiments that the grown seed size can be controlled by the arrangement of seed positions. The model is then used to optimize the seed positions for any desired output object to improve precision.

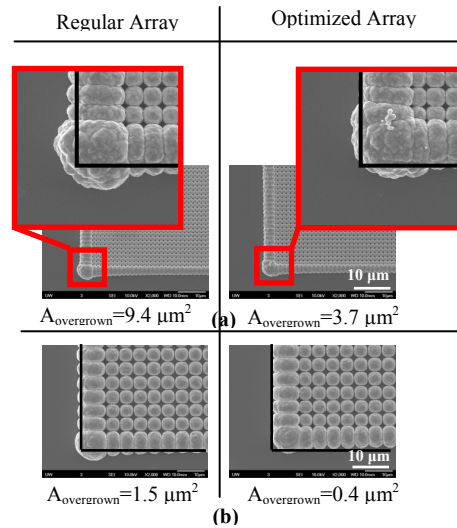


Figure 6: The regular square array (left) and the optimized array (right) are shown for (a) 250 nm seeds with 1.5 μm spacing and 12 seconds growth time, and (b) 500 nm seeds with 10 μm spacing and 60 seconds growth time. The optimized seeds show a sharper corner and a smaller overgrown area.

6. ACKNOWLEDGEMENTS

This work was supported by National Science Foundation grant CMMI 0709131 "NIRT: Protein-guided Nanomanufacturing". Part of this work was conducted at the University of Washington NanoTech User Facility, a member of the NSF National Nanotechnology Infrastructure Network (NNIN). We also thank Professor Vikram Jandhyala for inspiring discussions.

REFERENCES

- [1] Gates, B.D., Xu, Q., Stewart, M., Ryan, D., Willson, C.G., Whitesides, G.M., "New approaches to nanofabrication: Molding, printing, and other techniques", *Chemical Reviews*, v 105, n 4, p 1171-1196, 2005.
- [2] Chryssolouris, G., Tsoukantas, G., Salonitis, K., and Stournaras, A., "Nanomanufacturing Processes: A critical review", *International Journal of Materials and Product Technologies*, v 21, p 331-348, 2004.
- [3] Sarikaya, M., Tamerler, C., Jen, A. K. Y., Schulten, K. & Baneyx, F., "Molecular biomimetics: nanotechnology through biology", *Nature Materials*, v 2, p 577-585, 2003.
- [4] Bard, A.J., and Faulkner, L.R., "Electrochemical methods", *John Wiley*, 2000.
- [5] Stakgold, I., "Green's functions and boundary value problems", *John Wiley*, 1979.
- [6] Scharifker, B.R, Mostany, J. "Three-dimensional nucleation with diffusion controlled growth. Part 1", *J. electroanalytical chemistry*, v 177, n 1-2, p 13-23, 1984.